INVESTIGATION OF THERMAL CONDUCTIVITY OF IRON-SILICA MAGNETICALLY STABILIZED POROUS STRUCTURE

By

SAMAUN NILI

A THESIS PRESENTED TO THE GRADUATE SCHOOL
OF THE UNIVERSITY OF FLORIDA IN PARTIAL FULFILLMENT
OF THE REQUIREMENTS FOR THE DEGREE OF
MASTER OF SCIENCE

UNIVERSITY OF FLORIDA

2013

To my parents

ACKNOWLEDGMENTS

During the time I started my elementary school up to this moment of my graduate studies, I was helped and supported by many people which I like to thank them all for helping me to reach to this point where I am now. But I would like to specially thank my parents, which their endless engorgements and supports made this grate moment of success for me. My professors, Dr. Klausner , Dr. Mei and Dr. Abbitt, which gave me broad engineering knowledge which shall certainly guide me throughout my future professional courier. I also like to thank supervisor and my friends at the lab, Dr. Ayyoub Mehdizadeh, Amey Barde, Like Li, Nick AuYeung.

TABLE OF CONTENTS

page

LIST OF TABLES

LIST OF FIGURES

LIST OF ABBREVIATIONS

ETC	Effective Thermal Conductivity
EXP	Experimental
MSPS	Magnetically Stabilized Porous Structure
TC	Thermocouple
THW	Transient Hot Wire

NOMENCLATURES

Variables

C	Thermal heat capacity [J/Kg.K]
d	Diameter [m]
$\dot{g}$	Heat generation per unit volume [w/m^3]
i	Electrical current [A]
K	Thermal conductivity [W/K.m]
L	Length [m]
q	Heat flux [W]
R	Electrical resistance [Ω]
r	Radius [m]
T	Temperature [K]
t	Time [s]
V	Voltage [v]

Greek letters

α	Thermal diffusivity [m^2/s]
γ_{Eu}	Euler's constant
δ	Thickness [m]
θ	Angle [degree]
ρ	Density [Kg/m^3]

Subscripts

i	insulation
l	per unit length
r	radial
ref	Reference
w	Wire

Abstract of Thesis Presented to the Graduate School
of the University of Florida in Partial Fulfillment of the
Requirements for the Degree of Master of Science

INVESTIGATION OF THERMAL CONDUCTIVITY OF IRON-SILICA MAGNETICALLY STABILIZED POROUS STRUCTURE

By

Samaun Nili

May 2013

Chair: James F. Klausenr
Major: Mechanical Engineering

It is a fact of experience that simulation of thermo-fluid properties of magnetically stabilized porous structure (MSPS) [1] measurement requires accurate value of thermal conductivity of structure. Therefore, there is a critical need for measurements of thermal conductivity of MSPS. The dramatic effect of magnetic field on the thermal conductivity of MSPS has not studied before. In this study, we have developed a new apparatus based on the transient hot-wire technique to obtain measurement of thermal conductivity of MSPS under different magnetic field orientations. The experimental results show that, when an external magnetic field of 65 G is applied perpendicular or parallel to a hot wire axis, the geometry of iron particles are constrained, such that the most thermal conductivity decreased 12 % compared to the one without any magnetic field. Then it was both numerically and experimentally verified that applying the magnetic field does not have any significant effect on the behavior of the propagation of heat in any direction. Therefore, it is concluded that the change in the thermal conductivity of MSPS is mainly due to the increase of porosity.

Thermal conductivity is measured by tracking the thermal pulse propagation induced in the sample by a heating source consisting of an 80 µm nichrome wire. One E type exposed thermocouple was used to measure the temperature variation in the media.

CHAPTER 1
INTRODUCTION AND LITERATURE REVIEW

1.1 Literature Review

The porous media enhances fluid flow mixing by increasing the contact surface area, so porous structures are an effective heat transfer enhancement technique. Due to importance of the application of porous structures, there is a huge motivation to study of the heat transfer characteristic in porous media. Catalyst and chemical particle beds, micro-porous heat exchangers (solid matrix), phase array radar systems, cooling of electronic components such as mirror in powerful lasers, industrial high temperature furnaces, packed bed regenerators, micro-thrusters, transpiration cooling, spacecraft thermal management systems, fixed-bed nuclear propulsion systems, combustors and many others [2-6] can be considered as the application of these structures.

1.1.1 Magnetically Stabilized Porous Structure (MSPS)

Ayyoub M. Mehdizade and James F. Klausner in 2012 [1] have investigated on enhancement of thermochemical hydrogen production using iron-silica MSPS. The MSPS is used as the reactive substrate for two step water splitting, hydrogen production process. The reactivity of the material has been kept intact by controlling and constraining the geometry of matrix particles inside the structure in a desirable manner by applying an external magnetic field (Figure 1-1). Their hydrogen production is higher than those who reported in open literature for two step water splitting process [1]. Their experimental and analytical study of reaction kinetics of the laboratory scale magnetically stabilized iron-silica porous structure and they indicated that, MSPS is very suitable for the industrial applications where the enhanced reaction rate is desired, and their proposed model can be used for the design of larger scale reactors [7].

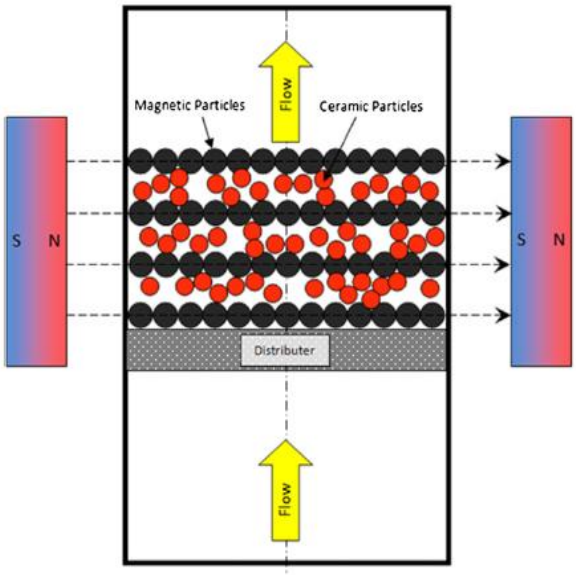

Figure 1-1. Schematic representation of the magnetically stabilized iron-silica porous structure [1]

1.1.2 Importance of Thermal Conductivity of Porous Structures

Recently, the porous structures have gained tremendous attention due to their wide industrial applications. Thermal conductivity is one of the major thermodynamic coefficients in the study of energy transport through porous Medias due to its applications in thermal energy storages devices, high temperature furnaces, bed catalyst, weather control, artificial heating and cooling of buildings, in geothermal operations, thermal exchange in heat pumps and energy conservation in buildings. Effective thermal conductivity (ETC) has been investigated extensively using both experimental and theoretical approaches by various scientists in detail [8].

1.1.3 Heat Transfer in a Packed Bed

The complex heat transfer phenomenon in packed beds with co current gas–liquid up-flow has been extensively investigated in the literature and several models have been developed in order to describe heat transfer in the bed. However, the

proposed correlations are valid in specific flow regimes only, for example: Nakamura, Tanahashi, Ohsasa and Suguyama (1981) studied the thermal conductivity of in pulsed flow, Sokolov and Yablokova (1983) studied the thermal conductivity of bubble flow, Gutsche, Wild, Roizard, Midoux and Charpentier (1989) and Lamine et al., 1992 and Lamine et al., 1992b studied the thermal conductivity of separated flow. Besides, most of these studies related to water (coalescent liquid) and air (or nitrogen) flow [9-13].

1.1.4 Previous Analytical Studies on ETC of Packed Beds

Numerous analytic models have been created and modified for achieving the ETC of packed beds in the presence of a static gas. As the examples, the models by Hall and Martin [14] referred to as ZBS. Three recent evaluations of a number of these models have been accomplished by Tsotsas and Martin [15], Fundamenski and Gierszewski [15], and Xu et al. [17]. The first two studies achieved that a reformed form of the ZBS model [13] did the best job of presenting the experimental data. The third study found serious absences with all three analytic models tested, and concluded that the UCLA two-dimensional, finite-element model [18] gave the most reliable predictions using reasonable parameters.

CHAPTER 2
CLASSIFICATION OF EXPERIMENTAL THERMAL CONDUCTIVITY MEASUREMENT

The value of thermal conductivity depends on temperature, compression, chemical composition, physical structure, state of substance. Moisture content also affects the thermal conductivity of a material. In fact there are many different techniques for measuring thermal conductivity. For limited range of materials, respecting to medium temperature and thermal properties, the proper technique has to be determined. A distinction can be made between steady-state and transient-state techniques.

2.1 Classification of Measurement Techniques

2.1.1 Steady State Techniques

When the material which is analyzed is completely at equilibrium, the steady-state techniques are generally performed. Requiring a long time to reach to equilibrium is one of the main disadvantages of this method. However, the signal analysis would be very easy since the steady state implies constant signals. In this method, thermal conductivity of medium is determined using temperature change and amount of heat flux across the surface. Thermal conductivity measurements using the steady state method are classified as a)horizontal flat plate method, b)vertical coaxial cylinder method, c)steady state hot-wire method d)method of concentric spheres, and e)absolute and relative methods.

2.1.2 Transient-State Techniques

Basically transient-state techniques are used when the thermal conductivity of the medium can be determined form the temperature response to heating. After an initial transition period, the raises in temperature of area close to the heater depend on just the thermal conductivity of the surrounding medium, and no linger on the heat

capacity of the wire. In transient methods there is no necessity of reaching a real thermal equilibrium while the medium is heating up. Transient-state techniques are fast and they are appropriate for quick measurements and they are suitable for field uses, as well. Typically in this method the temperature measurement is taken from (few centimeters away of the heater). In other transient hot wire techniques the temperature rise of the heater is measured in order to calculate thermal conductivity. Transient-state methods are classified as a)continuous line source (hot-wire) method, b)cylindrical source method, c)spherical source method, and d)plane source method. The present study is focused on the continuous line source method.

2.2 Classification of Hot-Wire Techniques

The THW is the well-established as the most reliable, robust and accurate technique [19] for evaluating thermal conductivity of fluids [20-22] and solids [23]. The difficulty of determining the establishment of the steady state condition, the difficulty in preventing natural convection, this transient hot wire method has been chosen in this study. In the transient hot wire technique if free convection is presented, it is easy to be detected because it will affect the linearity in the graph of temperature rise verses the logarithm of time. Transient hot-wire techniques are basically classified as the flowing:

2.2.1 Standard Cross Wire Method

On this technique, thermocouple is soldered or spot welded at the center of the wire which is already suspended in through the medium. An electric impulse passed through the wire and consequently, temperature rise due to the heating of the wire. The temperature rise in time is recorded by means of a thermocouple connected to the center of heat source. Typically, this method mostly used to measure thermal conductivity of solids, powders and rarely for fluids. Wild temperature measurement

range and proper temperature sensitivity are stated as the advantages for this method [24]. Due to the thermal contact resistance of the wire and thermocouple, some non-linearity errors occur during the measurement. When the direct current is applied to an asymmetrically arranged thermocouple, an error occurs to the temperature measurement, resulting in an increase or decrees of thermo-electric voltage, respecting to the polarity applied. These errors can be prevented by taking the mean of the primary and reversed applied DC voltage polarity measurements or either applying an alternative current.

2.2.2 Single Wire Resistance Technique

In this technique, a single wire can act as a both temperature sensor and heat source which has been submerge to the sample. The temperature rise in the wire is measured by the change of the resistance, caused by the heat source. The influence of local non-homogeneities is eliminated while measurement of the hot-wire mean temperature along its total or partial length [25]. In this method, cooling down of the wire by support, due to the finite length of the wire and finite axial boundary is suggested as a one of the main sources of error. The finite radius of the outer boundary, finite thermal conductivity of the wire, finite wire radius, and the finite head capacity of the wire can be classified as the other sources causing measurement error on this technique. However, these errors can be diminished by choosing an appropriate selection of hot-wire and dimensions of the wire cell. This could be stated as a straightforward technique for measuring thermal conductivity of electrically conductive material, if the above mentioned errors are compensated. This method has been performed for measuring the thermal conductivity of magnetically stabilized iron-silica porous structure in this study.

2.2.3 Potential Lead Wire Technique

The potential lead wire technique is a modified version of single wire resistance method, in order to prevent the errors which are caused by the end effects. Two potential leads are connected to the hot-wire in a proper distance from the ends on this technique. The current of heating is passed through the ends, while the potential drop in the wire is measured across a known length using the potential leads. The measure lead wire are maintained at a smaller cross section compare to that of hot wire, in order to avoid any influence of connections [24]. This is inappropriate method of measurement for electrically conductive materials for the following reasons. First of all, difficulty in attaching the potential leads to the hot wire at the required distance from the ends due to having insulation coating [26]. The other reason is that, a dip in the axial temperature profile of the hot-wire caused by an alternative path for the heat flow created by the potential leads [27].

2.2.4 Parallel Wire Method

In this technique, in order to compensate the end error effect, two hot-wires of different length are incorporated in the opposite arms of the bridge [28]. The measurement section is considered by difference between the lengths of the two wires. Thus, this configuration allows us to have an absolute measurement by experimental elimination of the end effects. The end geometry of short and long wires should be match in order to have an accurate measurement. This considered as a major problem of this construction, since attaining to an ideal end connections is difficult. The other problem, though insignificant, is that the two wires should have identical uniform cross-section. Since the wire from the same wire spool may not have uniform cross-section,

thus, improper cancellation of the end effects due to the different heat dissipation of wires occurs [27].

2.3 Reason for Adapting Single Wire Technique

In the present study the single wire hot-wire method has been performed as the measurement instrument for iron-silica magnetically stabilized porous structure thermal conductivity measurement. Simplicity of operation and low cost of construction is one of the reasons for adapting this method. Moreover, we need a very uniform insolation coating on the metal wire, which is difficult to attain in the case of cross-wire and potential lead techniques due to connections on the hot-wire itself. In the two wire parallel technique, it is difficult to construct identical end geometries. In case of the single wire method, only one hot-wire is used. Instead of using the hot wire as a temperature sensor by itself, a thermocouple in a reasonable distance from the hot wire was used to monitor the temperature on this study. Connections are easily attainable. Moreover, end errors can be minimized by optimizing the cell design.

CHAPTER 3
PRINCIPLE OF ANALYSIS

3.1 Mathematical Analysis

Thermal conductivity is measured by tracking the thermal pulse propagation induced in the sample by a heating source consisting of an 80 μm nichrome wire. One E type exposed thermocouple was used to determine the temperature in the media (Figure 3-1). The heat impulse transferred to the wire between two observed times gives a temperature increment of 9 ºC in 350 seconds which is depend on thermal conductivity of the structure.

The line heat source solution for the problem of conduction in a single-phase fluid or solid is well known and classical. Let us consider a wire of finite diameter and infinite vertical extent embedded into the target single-phase sample.

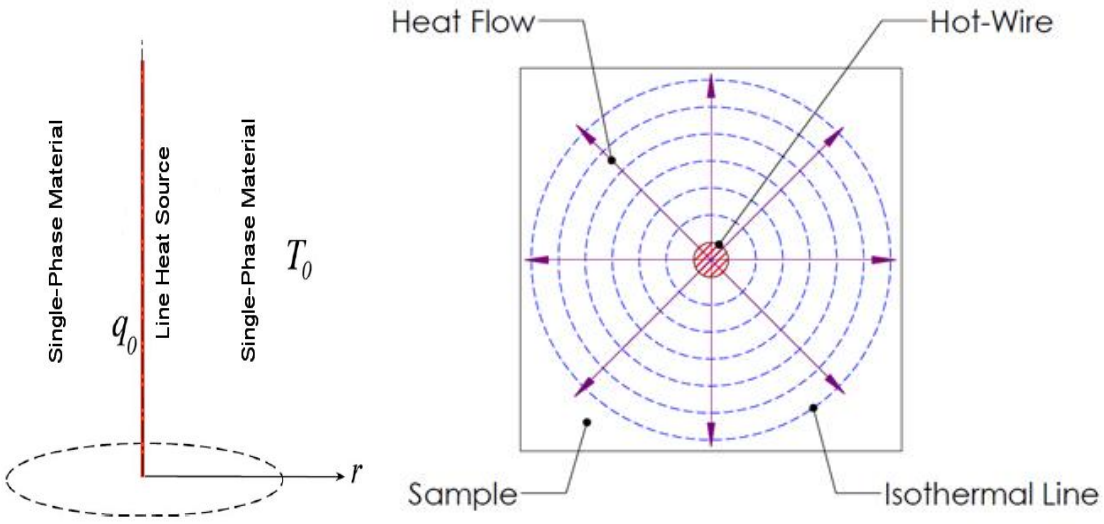

Figure 3-1. The line heat source analytical problem underlying the transient hot wire method

3.1.1 Governing Equations

The finite diameter is considered initially because it is more convenient to convert Ohm's heating parameters that are used in the transient hot wire method to a finite,

although very thin, wire diameter. Eventually the heat flux resulting from such a finite diameter wire will be evaluated in the limit when the wire radius tends to zero, thus converting it into the line heat source. The radius of this thin wire is taken as r_w, and the amount of heat generated per unit length (l) and of the nikrome wire by an electric current *i* [A] passing through the wire is $q_l = iV/l$ [W.m-1], Where V is the voltage implied to the wire. This heat rate per unit length generated within the wire by Ohm's heating can be converted into the corresponding amount of radial heat flux from the wire to the surrounding fluid or solid in the form Equation 3-1:

$$q_l = (q_r)_{r=r_w} \frac{2\pi r_w l}{l} = -2\pi r_w k \left(\frac{\partial T}{\partial r}\right)_{r=r_w} \quad (3\text{-}1)$$

Where q_r at $r = r_w$ is the radial heat flux from the wire.

The mathematical model for the hot-wire method is based on an ideal, infinitely long and thin continuous line source dissipating heat, of heat flux, q_l, per unit length, applied at time t = 0, in an infinite and incompressible medium. The general assumption is that heat transfer to the infinite medium of thermal conductivity k and thermal diffusivity $\alpha = k/\rho C$, is by conduction alone and thus increases both temperatures of the heat-source and test-medium with time. It is also assumed that the line heat-source has uniform instant temperature everywhere, but is transient in time (virtually achieved with small diameter and long wire with large thermal conductivity and/or small heat capacity). The governing equation is derived from the Fourier's equation for one-dimensional (1-D) transient heat conduction in cylindrical coordinates (Equation 3-2).

$$\frac{1}{\alpha}\frac{(\partial T)}{\partial t} = \frac{1}{r}\frac{\partial}{\partial r}(r\frac{\partial T}{\partial r}) \quad (3\text{-}2)$$

Where, $T = T_0 + \Delta T$ is the temperature of the medium at any time t and arbitrary radial distance r, T_0 is the initial temperature of the source and medium, and ΔT is the temperature difference between the medium and initial temperature. Equation 3-2 is the subject of the following boundary conditions (Equation 3-3 and Equation 3-4),

$$\lim_{r\to 0}\left\{r\left(\frac{\partial T}{\partial r}\right)\right\} = -\frac{q_l}{2\pi k} \qquad r = 0 \tag{3-3}$$

$$lim_{r\to 0}\{\Delta T(r,t)\} = 0 \qquad \text{at} \qquad t \geq 0 \text{ and } r \to \infty \tag{3-4}$$

Where ρ and C are density and specific heat capacity of the test medium, respectively. Solving for the radial heat conduction due to this line heat source leads to a temperature solution in the following closed form that can be expanded in an infinite series as follows (Equation 1-5) which is outlined by Carslaw and Jaeger [29].

$$T = \frac{q_l}{4\pi k} Ei\left(\frac{r^2}{4\alpha t}\right) = \frac{q_l}{4\pi k}\left[-\gamma_{Eu} + ln\left(\frac{4\alpha t}{r^2}\right) + \frac{r^2}{4\alpha t} - \frac{r^4}{64\alpha^2 t_2} + \frac{r^6}{1152\alpha^3 t_3} - \cdots\right] \tag{3-5}$$

Where $Ei(\bullet)$ represents the exponential integral function, and $\gamma_{Eu} = \ln(\sigma_{Eu}) = 0.5772156649$ is Euler's constant. After initial, short transient period (i.e. $t >> r^2/4\alpha$), except for the first term containing time t, the higher order terms could be neglected, resulting in a very good approximation as Equation 3-6 For a line heat source embedded in a cylindrical cell of infinite radial extent and filled with the test sample,

$$T \approx \frac{q_l}{4\pi k}\left[-\gamma_{Eu} + ln\left(\frac{4\alpha t}{r^2}\right) + O\left(\frac{r^2}{4\alpha t}\right)\right] \tag{3-6}$$

Equation 3-6 reveals a linear relationship, on a logarithmic time scale, between the temperature and time. Thus, one way of evaluating the thermal conductivity is from the slope of the above relationship evaluated at any fixed radial position. However, the latter needs the knowledge of thermal diffusivity of the sample.

There for, for constant sample medium properties and a fixed and arbitrary radius *r*, differentiation of Equation 3-6 shows that all dependence on radius, *r*, is lost and the following relation is obtained (Equation 3-7).

$$(T_2 - T_1) \approx \frac{iV}{4\pi kl}\left[\ln\left(\frac{t_2}{t_1}\right)\right] \qquad (3\text{-}7)$$

There for, the thermal conductivity can be obtained by rearranging Equation 3-6 as below (Equation 3-8):

$$k \approx \frac{iV}{4\pi(T_2 - T_1)l}\left[ln\left(\frac{t_2}{t_1}\right)\right] \qquad k \approx \frac{q_L}{4\pi}\frac{1}{d(\Delta T)/dln(t)} \qquad (3\text{-}8)$$

Therefore, if temperature of the medium is measured as function of time at any fixed radial position, including at the point of contact with the line source (i.e. the temperature of the thin line source) which can be found by measuring the changes of the electrical resistance of the line heat source, the thermal conductivity of the test medium, *k*, is proportional to the source heat flux and inversely proportional to the temperature (or temperature difference) gradient with regard to the natural logarithm of time.

3.1.2 Application of Hot-Wire Technique for Porous Structures

Typically, a bare metal wire which is centered in a sample is used for thermal conductivity measurement of the samples. Since the sample contains iron particles which are electrically conductive, there for ambiguous results in the measurements will appear due to application of bare wire. Some common problems which identified by Nagasaka and Nagasahima [26] in the application of ordinary transient hot wire technique to electrically conductive liquids are:

- Resulting of ambiguous measurement of generated heat in the wire due to possible current flow through the liquid
- Polarization of the wire surface

- Distortion of output voltage signal due to the conducting liquid cell

Using an electrically insulating material in order to overcome these errors is recommended. The study of thin insulation on temperature distribution has been performed by Nagasaka and Nagashima [26] and outlined by Yamasue et al. [30]. The temperature rise of hot wire is given as Equation 3-9,

$$(\Delta T) \approx \frac{q_l}{4\pi k}\left[\ln t + A_0 + \frac{1}{t}(B_0 lnt + C_0)\right] \tag{3-9}$$

Where A_0, B_0 and C_0 are defined as below (Equations 3-10, 3-11, 3-12):

$$A_0 = \ln\left(\frac{4\alpha}{r_0^2\gamma}\right) + \frac{2k}{k_i} ln\frac{r_0}{r_w} + \frac{k}{k_w} + \cdots \tag{3-10}$$

$$B_0 = \frac{1}{2k}\left\{r_w^2\left(\frac{k}{\alpha_i} - \frac{k_w}{\alpha_w}\right) + r_0^2\left(\frac{k}{\alpha_f} - \frac{k_i}{\alpha_i}\right)\right\} \tag{3-11}$$

$$C_0 = \frac{r_w^2}{8}\left\{\left(\frac{k-k_i}{k_w}\right)\left(\frac{1}{\alpha_w} - \frac{1}{\alpha_i}\right) + \frac{4}{\alpha_i} - \frac{2}{\alpha_w}\right\} + \frac{r_0^2}{2}\left(\frac{1}{\alpha} - \frac{1}{\alpha_i}\right)$$
$$+ \frac{r_w^2}{k_i}\left(\frac{k_i}{\alpha_i} - \frac{k_w}{\alpha_w}\right)\ln\left(\frac{\mathrm{r_0}}{\mathrm{r_w}}\right) \tag{3-12}$$
$$+ \frac{1}{2k}\left\{r_w^2\left(\frac{k_i}{\alpha_i} - \frac{k_w}{\alpha_w}\right) + r_0^2\left(\frac{k}{\alpha} - \frac{k_i}{\alpha_i}\right)\right\}\ln\frac{4\alpha}{r_0^2\gamma}$$

Where, r_0 is the sum of the radius of the wire r_w and the insulation thickness δ_i. Subscripts w and I represent wire and insulation, respectively.

Comparison between equations 3-7 and 3-9 shows that the term $(1/t)(B_0 \ln t + C_0)$ is because of the existence of the insulation on the wire. Thus, the plot of ΔT verses $\ln(t)$ will shifted without changing the slope by the constant of A_0 if the term $(1/t)(B_0 \ln t + C_0)$ is negligibly small in comparison with the $(\ln t + A_0)$.

Electrical insulation coating to bare metal wire has been recommended for electrically conducting fluids. Nagasaka and Nagashima have coated the platinum wire (diameter

40 μm) with polyester insulation (thickness 7.5 μm) to measure electrically conducting aqueous NaCl solution [26]. While Perkins anodized a tantalum wire (diameter 25.4 μm) to form an electrically insulating layer of tantalum peroxide (thickness 70 nm) [31], Yu et al. have used an epoxy insulation coating (estimated thickness 10 μm) on a platinum wire (diameter 76.2 μm) in order to measure thermal conductivity of nanofluids [32]. Jwo et al. [33] insulated a Nickel-Chromium alloy wire with Teflon to measure thermal conductivity of CuO nanofluids. Recently, Ma in his thesis has utilized a platinum wire (diameter 25 μm) with an Isonel insulation coating (thickness 1.5 μm) for measuring thermal conductivity of various combinations of nano crystalline material and base fluids [34].

3.2 Hot-wire Apparatus Design

The present design has been conceptualized to provide a flexible method to easily replace the sample and disassemble the cell to clean the parts. Some of the important design factors that have been considered are: flexibility in handling and cleaning, centering of the platinum hot-wire, connections of the leads to the hot-wire, electrical wire routing, temperature measurement of the sample, and electrical and signal wiring connections.

The main design parameters are: (a) material of hot-wire, (b) radius of hot-wire, (c) insulation tube, (d) length of hot-wire, (e) radius of the test sample outer boundary, and (f) length of the sample.

Nichrome has been selected as superior hot wire material. It has higher thermal conductivity (TC) compared to the tantalum, also used as hot-wire. Along with the material, hot-wire radius is one of the most important parameters for the cell design. Among commercially available sizes, 80-μm radius platinum-wires have been selected

for the present application, since smaller 12.5-μm is considered to be too fragile for cleaning and handling of micro particle samples and it also provide a desirable value of resistance in compare to the internal resistances.

A 1/16 inches ceramic tube has been selected as insulating material, as it is highly resistant to electric conduction, chemical reactions, corrosion and stress-cracking at high temperatures. An 80-μm diameter nichrome wire with a ceramic insulation tube of 0.44 mm thickness, has been used as the hot-wire.

In this design, the length of the nichrome hot-wire (L_w) was taken as 0.15 m. The hotwire cell outer boundary radius was determined as 49mm. The overall sample volume V_c after fabrication is calibrated to be 246 mL. A cross sectional view of the newly designed hotwire thermal conductivity apparatus is shown in Figure 3-2.

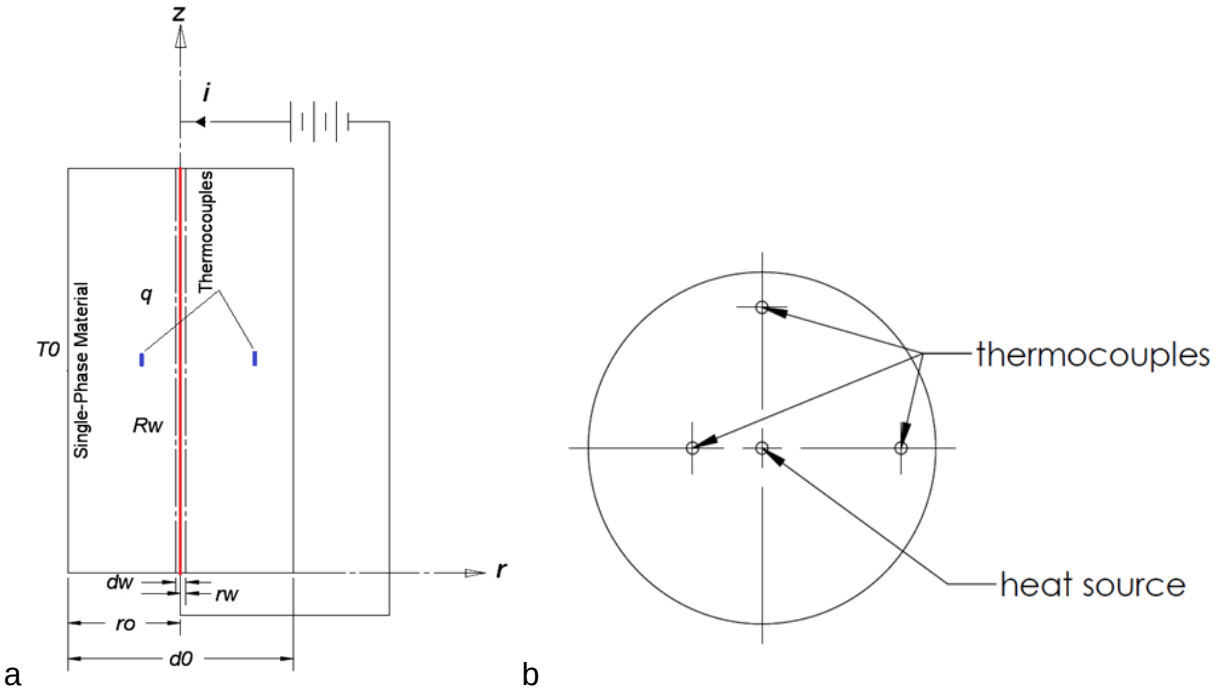

Figure 3-2. Schematic representation of the transient hot wire experimental setup. A) Front view. B) Top view of the hot wire cell which represents thermocouples and heat source position.

Figure 3-3. Experimental setup for THW experiment. Photo courtesy of Nili,S.

where r_0, d_0, r_w, d_w, T_0, R_w ,L and q represent the radius of the cell, diameter of cell, radius of the thin wire, diameter of the thin wire, distance between the magnets room temperature, electrical resistance of the wire and heat flux, respectively.

The major assembly components of the apparatus cell are: base plate, outer shell, and cell caps with hot-wire. The cell base plate with five threaded holes at the center and corners of the plate is used for convenient assembling and disassembling the outer shell. The outer quartz shell with 46 mm inner diameter acts as the sample test particles reservoir. The Teflon cell caps, designed and fabricated to slide-fit into the outer shell, are hollow inside. The inner three thermocouples, mounted on the inside of the tube, monitor the test particles temperature. Even though in this technique only one thermocouple is required for evaluation of thermal conductivity, the second thermocouple is added to the system in order to crosscheck the calculated thermal conductivity from the temperature history. The third thermocouple, orthogonal to the second thermocouple is added as well in order to see whether there is uniform heat flux in azimuthal direction.

All temperature measurements are controlled using the LabVIEW® 2011 user interface and NI USB-6211 data acquisition with a hot-wire power supply (14602ps MPJA) as and a multimeter (T&M ALLIANCE) for measuring the amp and voltage of the hot-wire with the resolution of 10 mV and 1 mA.

All thermocouples are calibrated using a high resolution thermometer and we used a thermistor glass 10K OHM D0-35 AL03006-5818-97-G1 as the cold junction compensation in order to have more accurate measurement.

Three E-type thermocouples are embedded in the 9.1 mm and 18.3 mm in the mixture of the iron-silica particles with the size range of 63-75 and 75-105 μm, respectively. Table 3-1 lists the dimensions of the experimental set up while Figure 3-4 experimental apparatus. The thermal conductivity under two different magnetic fields orientation has been investigated (Figure 3-6).

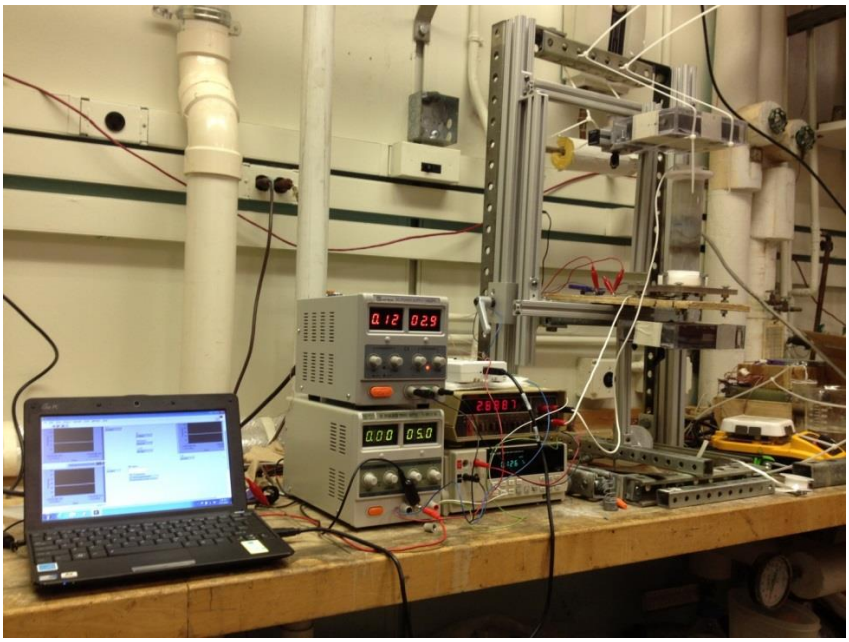

Figure 3-4. Experimental setup while there is a vertical magnetic field. Photo courtesy of Nili, S.

Table 3-1. Geometry of apparatus

R_w Ω	d_w mm	r_w mm	d_o mm	r_o mm	r_1 mm	r_2 mm	L mm
20.631	3.1	1.5	45.7	22.8	9.1	18.3	300

The fixture in Figure 3-4 was made in a way to provide three degree of freedom for each magnet. Thus the desire magnetic field properties can be easily achieved.

3.3 Sample Preparation

The 63-75 micron 99.65% purity iron particles mixed with 75-105 micron silica particles with volume ratio of ½ has been used for this experiment. Two magnets have been used in order to stabilize the structure while it was being fluidized. Table 3-2 shows the sample physical material properties before and after mixing. The iron-silica chains can be easily detected in Figure 3-5 D.

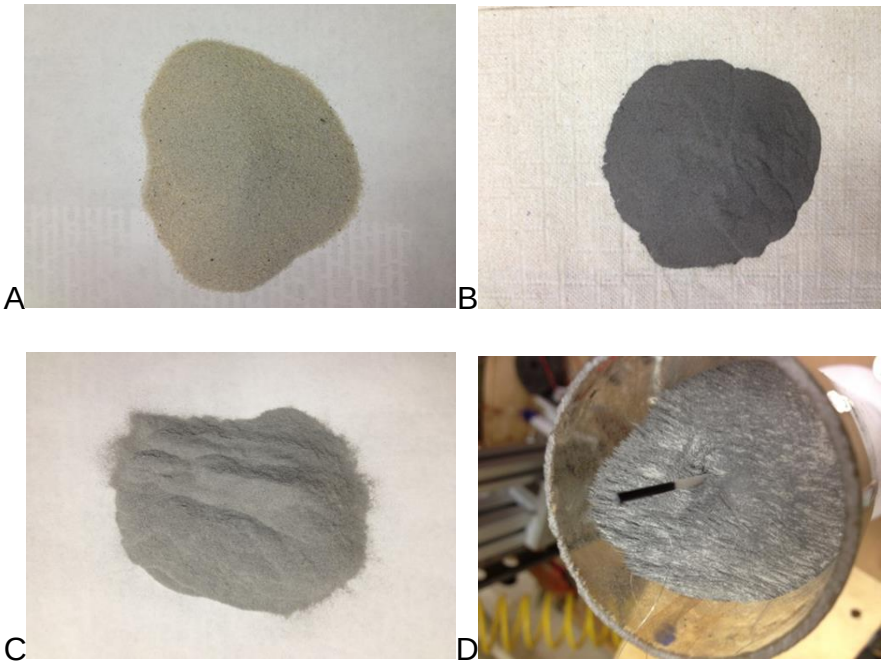

Figure 3-5. The powders and mixture. A) Silica particles B) Iron particles. C) Iron-silica parties before stabilizing. D) magnetically stabilized iron-silica packed bed. Photo courtesy of Nili, S.

Table 3-2. Material physical properties

	Size range	Material density	Powder apparent density	Mass powder	Porosity	Thermal heat capacity
	mm	g/cm^3	g/cm^3	g	%	J/g-K
Iron	63-75	7.87	2.81	275.80	63	0.703
Silica	75-105	2.65	1.55	230.00	41	0.450
Mixture			1.89	505.8	53	0.565

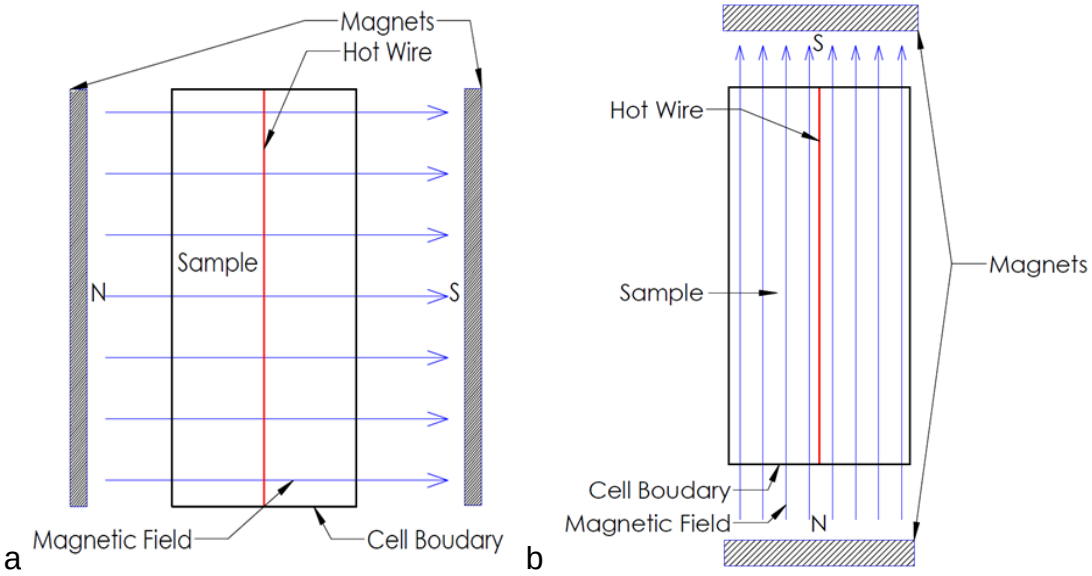

Figure 3-6. Typical schematic setup for the transient hot wire experiment. A) With horizontal magnetic field. B) With vertical magnetic field.

3.4 Measurement Process

All temperature measurements are controlled using the LabVIEW® 2011 user interface and NI USB-6211 data acquisition with a hot-wire power supply (14602ps MPJA) and a multimeter (T&M ALLIANCE) for measuring the amp and voltage of the hot-wire with the resolution of 10 mV and 1 mA. All thermocouples are calibrated by using a high resolution thermometer and a thermistor glass 10K OHM D0-35 AL03006-5818-97-G1 was used as the cold junction compensation in order to have an accurate measurement. Thermal conductivity measurements of the sample under each condition have been repeated 2 times. The time range from 250 to 750 s has been determined to

be linear, (Figure 3-8). The reference temperature T_{ref} , at which magnetic field orientation measured, is evaluated as the process average temperature (Equation 3-13).

$$T_{ref} = T_0 + \frac{1}{2}[\Delta T(t_1) + \Delta T(t_2)] \qquad (3\text{-}13)$$

Where $\Delta T(t_1)$ and $\Delta T(t_2)$ are corresponding to temperature rises at t_1 and t_2 respectively.

The powder temperature are measured by three E-type thermocouples with respect to time is shown in Figure 3-7. Due to the transient nature of the experiment, thermal conductivity is measured using exposed thermocouples. It is expected that the results of the exposed thermocouple are more accurate due to its smaller time constant. After passing a transition region, the temperature rise falls in a linear fashion for both of the thermocouples (Figure 3-8 and Figure 3-9). Next, measurements were repeated for different heat fluxes and as expected the ratio of the heat flux verses the slope of temperature-log of time remains constant. Then the same experiments were repeated while the system was exposed to the vertical and horizontal magnetic field shown in (Figure 3-8 and Figure 3-9) with a magnetic flux density of 65 gausses.

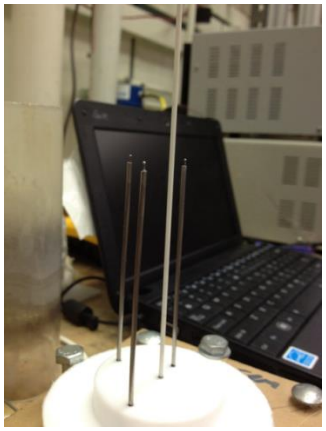

Figure 3-7. Thermocouples and heat source position. Photo courtesy of Nili, S.

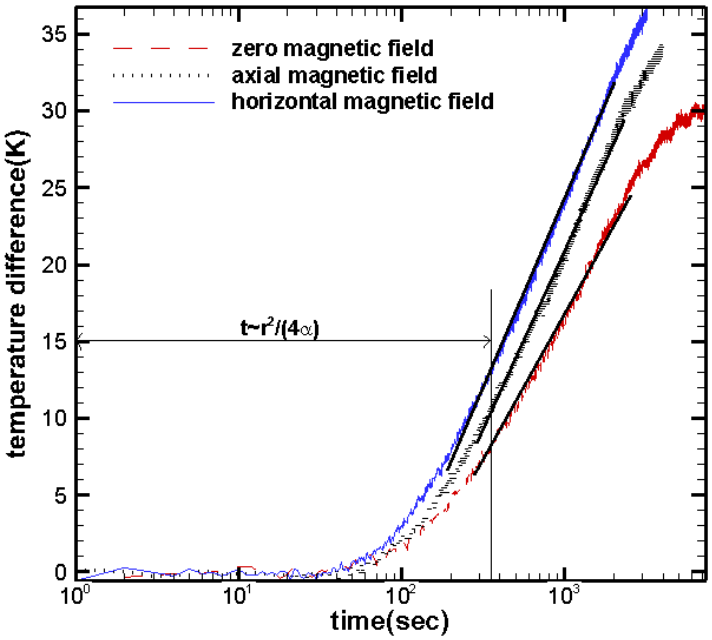

Figure 3-8. Temperature raise vs. time in log scale with 3.9 watts heat flux for different magnetic field orientations

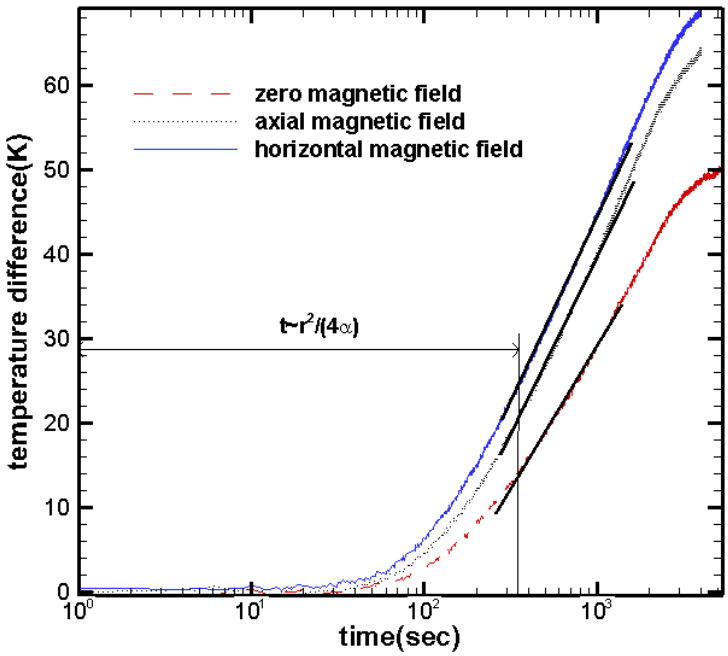

Figure 3-9. Temperature raise vs. time in log scale with 7.3 watts heat flux for different magnetic field orientation

3.5 Results

For 2:1 silica/iron mixture ratio, the experimental results showed that, when the magnetic field direction was perpendicular to the hot wire axis, the maximum thermal conductivity reduction was 12% in comparison to the case without any magnetic field. It was suggested that the magnetic field organized the iron chains in the normal direction of hot wire surface and repulsive force between chains, increases the structure porosity. Both of these effects will limit the heat flux penetration from the hot wire to the media and results in a lower thermal conductivity. In the other hand, when the magnetic field switched to the parallel direction to hot wire axis, the radial thermal conductivity decreased by 11 % due to decreased contact between iron particles in the radial direction. Tables 3-3 to 3-5 and Figures 3-10 to 12 show the calculated value of thermal conductivity of the material with/without magnetic field. The raw experimental data was recorded from exposed E-type thermocouple for two different amounts of heat fluxes.

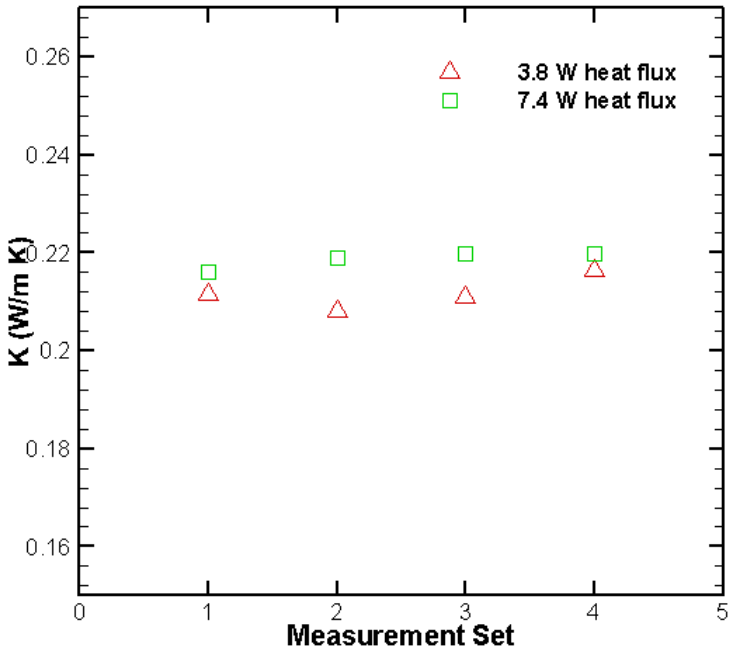

Figure 3-10. Thermal conductivity of iron-silica powder while there is no external magnetic field for porosity of 57.8 %

Table 3-3. Thermal conductivity measurement of mixture without magnetic field

Experiment number	mass (g)	Power (W)	Porosity (%)	Thermal Conductivity (W/m K)
1	439.3386	3.77	57.8	0.211
2	439.3386	3.77	57.8	0.208
3	439.3386	3.78	57.8	0.211
4	439.3386	3.77	57.8	0.216
1	439.3386	7.36	57.8	0.216
2	439.3386	7.34	57.8	0.219
3	439.3386	7.35	57.8	0.220
4	439.3386	7.34	57.8	0.220

Thermal conductivity of the sample without any magnetic field for two different heat fluxes are shown in Table 3-3 and Fig 3-10 for four measurement sets.

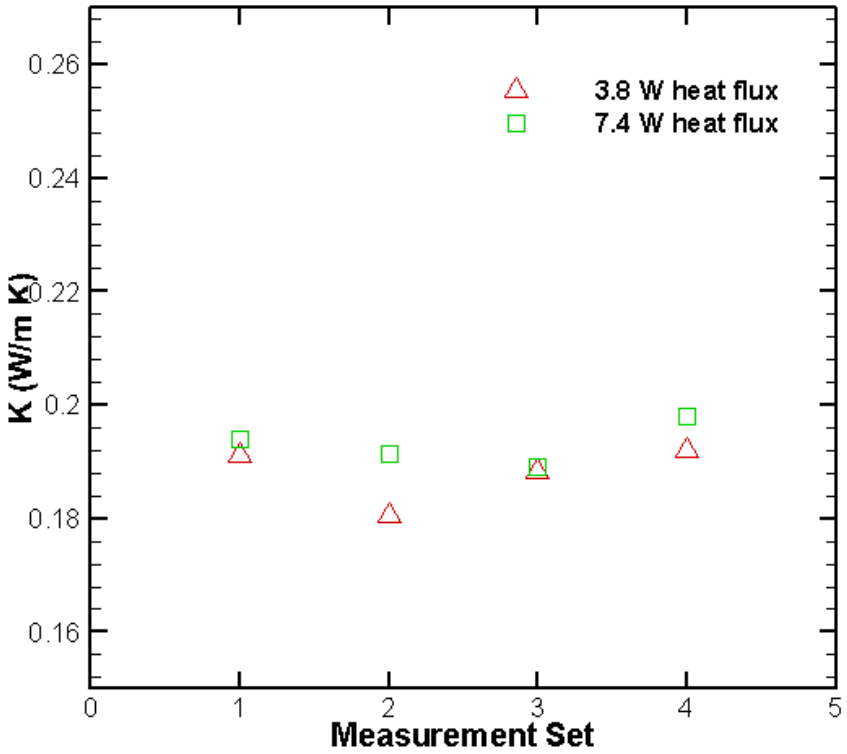

Figure 3-11. Thermal conductivity of iron-silica powder while there is a 65 G horizontal external magnetic field vs. experiment number for porosity of 62.9 %

Table 3-4. Thermal conductivity measurement of iron-silica porous structure while there is an 65 G horizontal external magnetic field

Experiment number	mass (g)	Power (W)	Porosity (%)	Thermal Conductivity (W/m K)
1	402.1074	3.76	62.9	0.188
2	402.1074	3.72	62.9	0.192
3	402.1074	3.76	62.9	0.191
4	402.1074	3.76	62.9	0.181
1	402.1074	7.36	62.9	0.194
2	402.1074	7.36	62.9	0.192
3	402.1074	7.37	62.9	0.189
4	402.1074	7.31	62.9	0.198

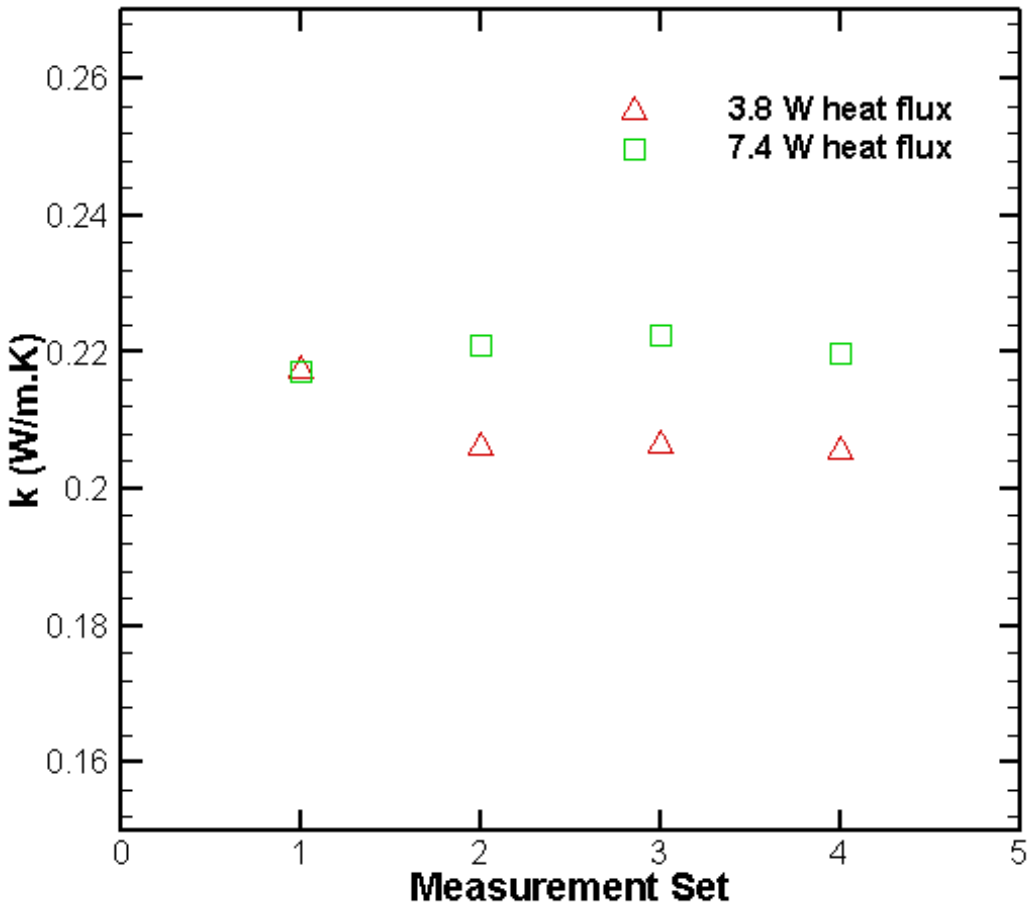

Figure 3-12. Thermal conductivity of iron-silica powder while there is a 65 G horizontal external magnetic field vs. experiment number for 59.5 % of porosity

Table 3-5. Thermal conductivity measurement of iron-silica porous structure while there is a 65 G horizontal external magnetic field

Measurement set	mass (g)	Power (W)	Porosity (%)	Thermal Conductivity (W/m K)
1	439.33	3.86	59.5	0.217
2	439.33	3.82	59.5	0.206
3	439.33	3.81	59.5	0.207
4	439.33	3.79	59.5	0.206
1	439.33	7.38	59.5	0.217
2	439.33	7.38	59.5	0.221
3	439.33	7.35	59.5	0.223
4	439.33	7.32	59.5	0.219

Thermal conductivity of the sample with 65 G external horizontal magnetic field for two different heat fluxes and porosities have been shown in Table 3-4, Figure 3-11, Table 3-5 and Figure 3-12 report the measured data for four measurement sets.

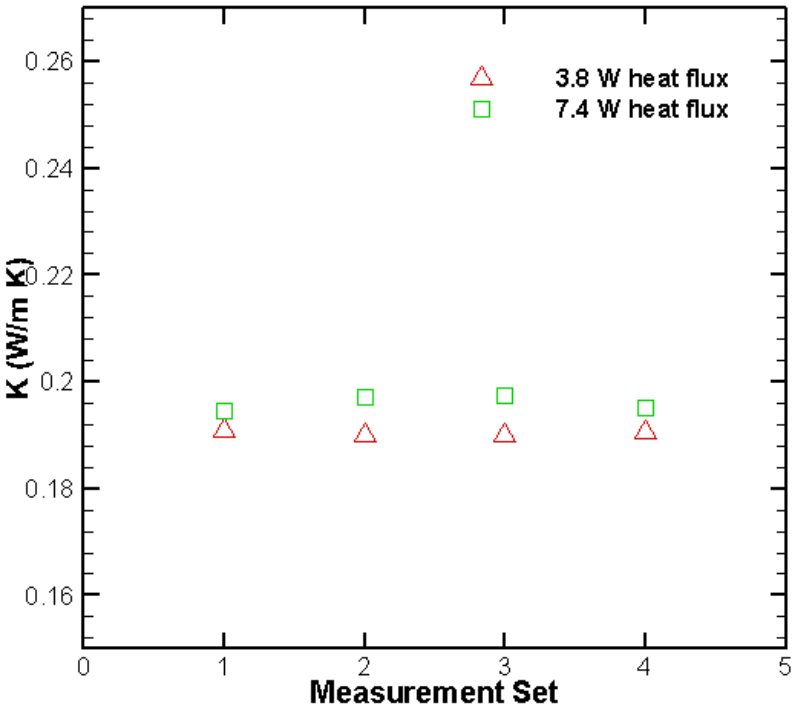

Figure 3-13. Thermal conductivity of iron-silica powder while there is a 65 G vertical external magnetic field vs. experiment number for 62.9 % of porosity

Table 3-6. Thermal conductivity measurement of iron-silica porous structure while there is a 65 G vertical external magnetic field

Experiment number	mass (g)	Power (W)	Porosity (%)	Thermal Conductivity (W/m K)
1	402.1074	3.84	62.9	0.191
2	402.1074	3.84	62.9	0.190
3	402.1074	3.84	62.9	0.190
4	402.1074	3.83	62.9	0.191
1	402.1074	7.45	62.9	0.194
2	402.1074	7.45	62.9	0.197
3	402.1074	7.45	62.9	0.197
4	402.1074	7.42	62.9	0.195

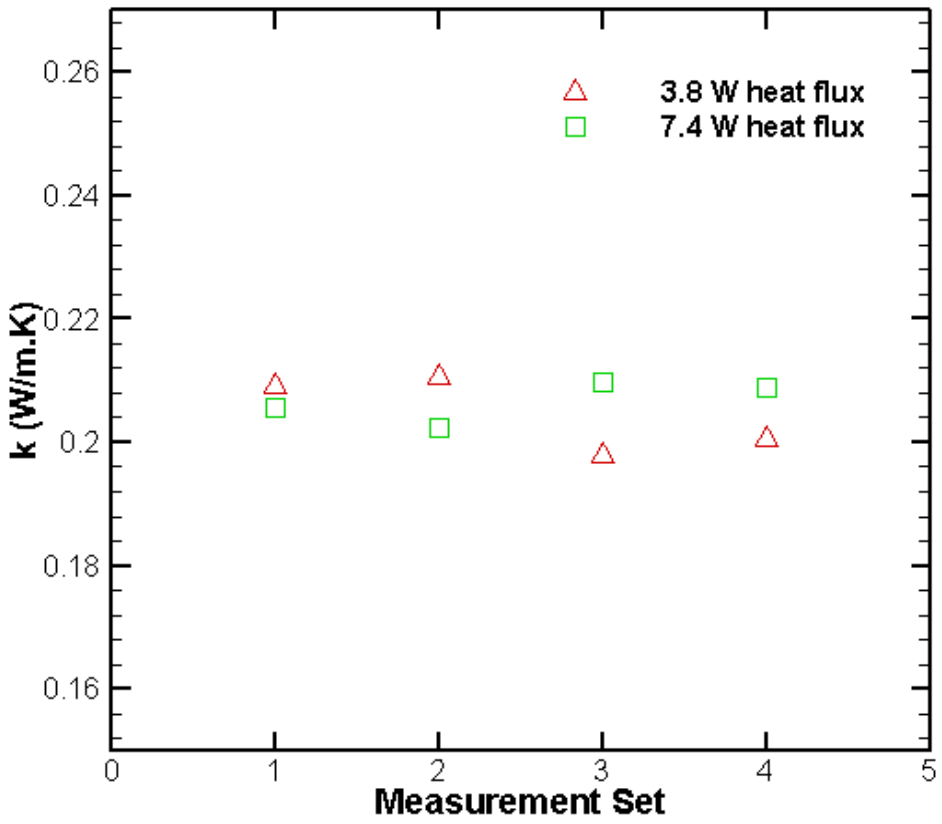

Figure 3-14. Thermal conductivity of iron-silica powder while there is a 65 G vertical external magnetic field vs. experiment number for 59.5 % of porosity

Table 3-7. Thermal conductivity measurement of iron-silica porous structure while there is a 65 G vertical external magnetic field

Measurement set	Mass (g)	Power (W)	Porosity (%)	Thermal Conductivity (W/m K)
1	439.33	3.77	59.5	0.206
2	439.33	3.97	59.5	0.211
3	439.33	3.76	59.5	0.195
4	439.33	3.78	59.5	0.197
1	439.33	7.34	59.5	0.206
2	439.33	7.35	59.5	0.202
3	439.33	7.34	59.5	0.210
4	439.33	7.32	59.5	0.209

Thermal conductivity of the sample with 65 G external vertical magnetic field for two different heat fluxes and porosities have been shown in Table 3-6, Figure 3-13, Table 3-7 and Figure 3-14 report measured data for four measurements set.

To summerize in Figure 3-15, Table 3-8, Figure 3-16 and Table 3-9 the average of four experimental measurements of thermal conductivity in different heat fluxes, porosities and magnetic field orientations are shown respectively.

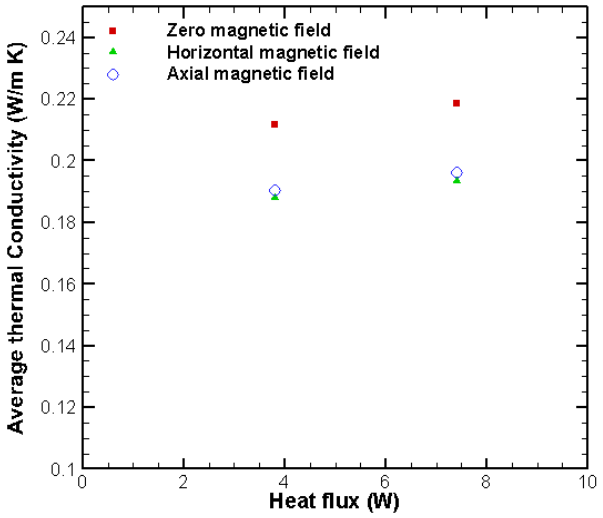

Figure 3-15. Average thermal conductivity of iron-silica porous structure for different heat fluxes and magnetic field orientations

Table 3-8. Average thermal conductivity of iron-silica porous structure for different heat fluxes and magnetic field orientations

Heat flux (W)	Average thermal conductivity without magnetic field (W/m K)	Average thermal conductivity with horizontal magnetic field (W/m K)	Average thermal conductivity with vertical magnetic field (W/m K)
3.8	0.212	0.188	0.190
7.4	0.211	0.193	0.196

In Figure 3-13 and Table 3-6 we have the porosity of 57.8 % and 62.9 % for the case that there is no external magnetic field and while there is horizontal/vertical magnetic field respectively. Figure 3-17 compares thermal conductivity of magnetically stabilized silica iron powder for two different porosities and magnetic field orientations.

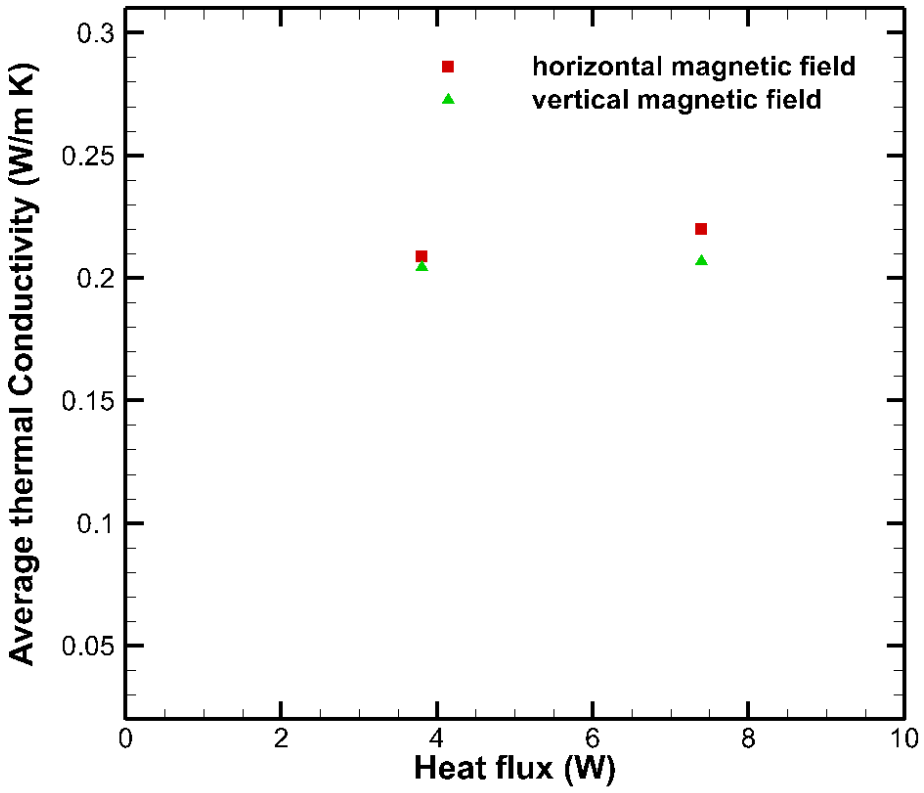

Figure 3-16. Average thermal conductivity of iron-silica porous structure for different heat fluxes and magnetic field orientations and porosity of 59.5 %

Table 3-9. Average thermal conductivity of iron-silica porous structure for different heat fluxes and magnetic field orientations and porosity of 59.5 %

Heat flux (W)	Average thermal conductivity with horizontal magnetic field (W/m K)	Average thermal conductivity with vertical magnetic field (W/m K)
3.8	0.209	0.204
7.4	0.220	0.207

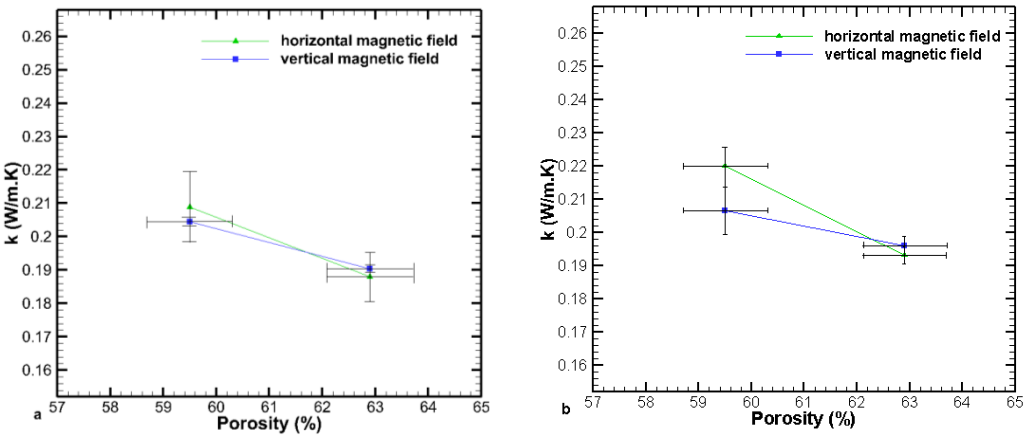

Figure 3-17. Average thermal conductivity measurement of iron-silica porous structure with vertical and horizontal magnetic field for different porosities. A) 3.8 watts heat flux. B) 7.4 Watts heat flux.

CHAPTER 4
NUMERICAL SIMULATION OF HEAT TRANSFER ON IRON-SILICA POURS STRUCTURE

4.1 Overview

In this chapter magnetically stabilized iron-silica porous structure has been numerically simulated in order to validate the experimental measurement results and also confirm there is a uniform radial heat flux in our sample. Thus, a computer code y using Fortran 90 has been created and developed and the results have been shown by utilizing the Tecplot 360, 2012 software.

4.1.1 Validating the Experimental Measurements Using the Numerical Simulation of Heat Transfer on Iron-Silica Pours Structure

In this section a numerical curve was fitted on our experimental data to validate our measurements. For this purpose, an energy balance equation is used for each element by using explicit finite volume method for iron-silica pours structure once we do not have any external magnetic field and for the case which there is a horizontal external magnetic field perpendicular to the hot wire surface (Figure 4-1 and Equation. 4-1).

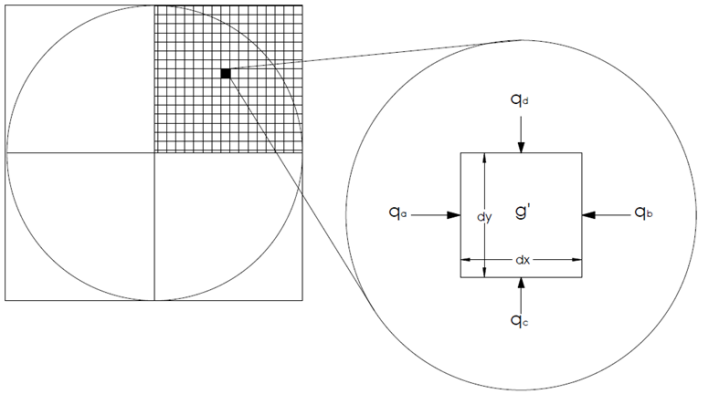

Figure 4-1. Schematic representation of heat balance for a control volume, advantage of symmetry boundary condition used, half sized meshes used for boundary edges.

$$
\begin{aligned}
\langle q_a \rangle &= \langle k * \frac{dy}{dx} * \langle previousTemp_{m-1,n} - previousTemp_{m,n} \rangle \rangle \\
\langle q_b \rangle &= \langle k * \frac{dy}{dx} * \langle previousTemp_{m+1,n} - previousTemp_{m,n} \rangle \rangle \\
\langle q_c \rangle &= \langle k * \frac{dx}{dy} * \langle previousTemp_{m,n-1} - previousTemp_{m,n} \rangle \rangle \\
\langle q_d \rangle &= \langle k * \frac{dx}{dy} * \langle previousTemp_{m,n+1} - previousTemp_{m,n} \rangle \rangle \\
\langle q_d \rangle &= \langle k * \frac{dx}{dy} * \langle previousTemp_{m,n+1} - previousTemp_{m,n} \rangle \rangle \\
&\langle CurrentTemp_{m.n} \rangle \\
&= \langle k * \frac{dx}{dy} * \langle previousTemp_{m,n} \rangle + \langle \frac{dt}{dx * dy * Cp} \rangle \\
&* \langle q_a + q_b + q_c + q_d + g \cdot \rangle \rangle
\end{aligned}
\tag{4-1}
$$

Where q_i (i=a,b,c,d), dx, dy, dt, g are representing the amount of heat flux which is comes through the element from each direction, element size, time step, amount of heat generated per unit length respectively and previousTemp and currentTemp are regarding to the element temperature in two different time steps, m and n subscripts are representing the element location. Figure 4-2 shows the analytical solution from equation 3-5 and a numerical curve fitted on our experimental data and we can see that all our measurements falls on a straight line in logarithmic scale for first 750 seconds which is enough time for having reliable measurements. After passing this time, the numerical curve departs from the experimental measurements, indicating that the transient method is no longer valid and the temperature distribution is approaching to an asymptotic steady state condition. The analytical solution in Figure 4-2 also shows lower ($t >> r^2/4\alpha$) and upper bound (750 sec) for valid measurement and it can be seen that the upper bound for both analytical and numerical simulation are the same. Therefore, this model is valid only for the first 750 seconds in our experiment.

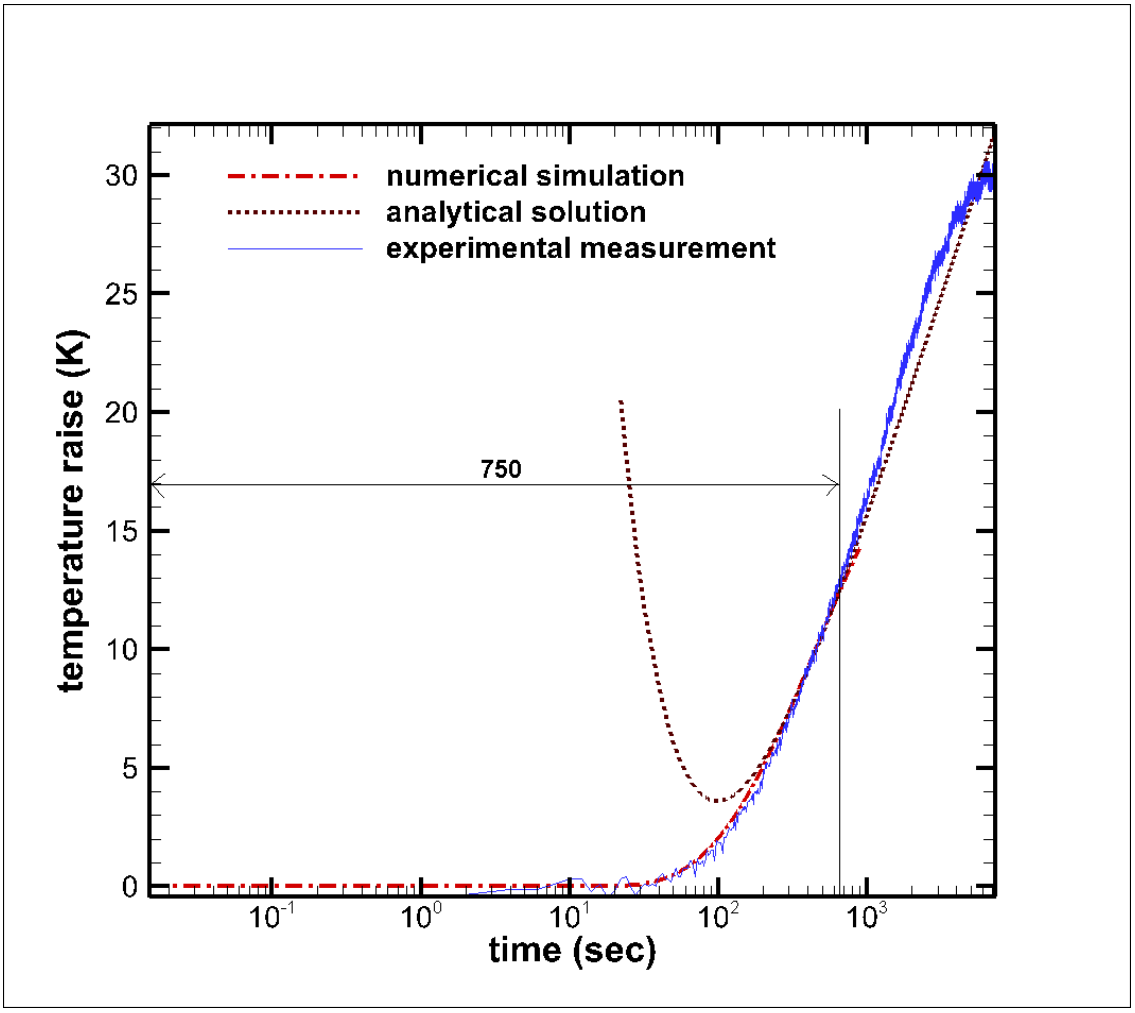

Figure 4-2. Comparison between numerical simulation and experimental measurements for homogeneous mixture of iron-silica powder in experiment 1 without external magnetic field

4.1.2 Numerical Simulation of Heat Distribution for Anisentropic Medium

Now we investigate the heat flux and temperature distribution along the azimuthal direction while the media is anisotropic and consisting of two arbitrarily materials with different thermal conductivities of k_1 and k_2.

It was initially expected that the heat flux and temperature distribution are not identical at the location of thermocouples 1 and 2 (shown in Figure 4-3a) due to different thermal resistances when two different materials with conductivity of k_1 and k_2

appeared frequently in the structure (Figure 4-3a 4-3b). Note that in all Figure 3-4, the total volumes of material 1 and 2 are kept unchanged and the only difference in the structure is their frequency of appearance. The mesh study is performed in order to ensure the high accuracy of simulation is achieved. Figure 4-4 shows the temperature as a function of time with different grid resolutions for the highest frequency of appearance in our study. It shows that the results are grid independent when more than 200 uniform grids are used in each direction for the highest simulated frequency of the appearance; the material 1 and 2 include 3 and 6 grids, respectively.

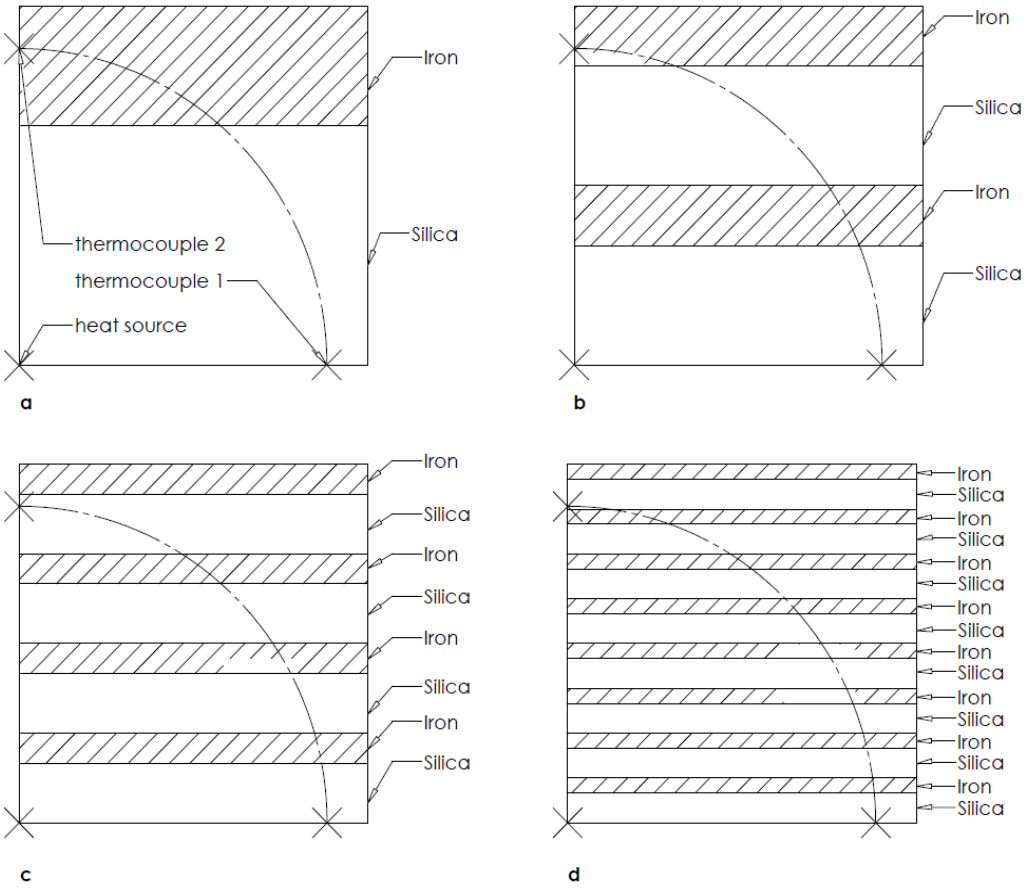

Figure 4-3. Frequency of iron-silica chains appearance when the sample is exposed to horizontal magnetic field.

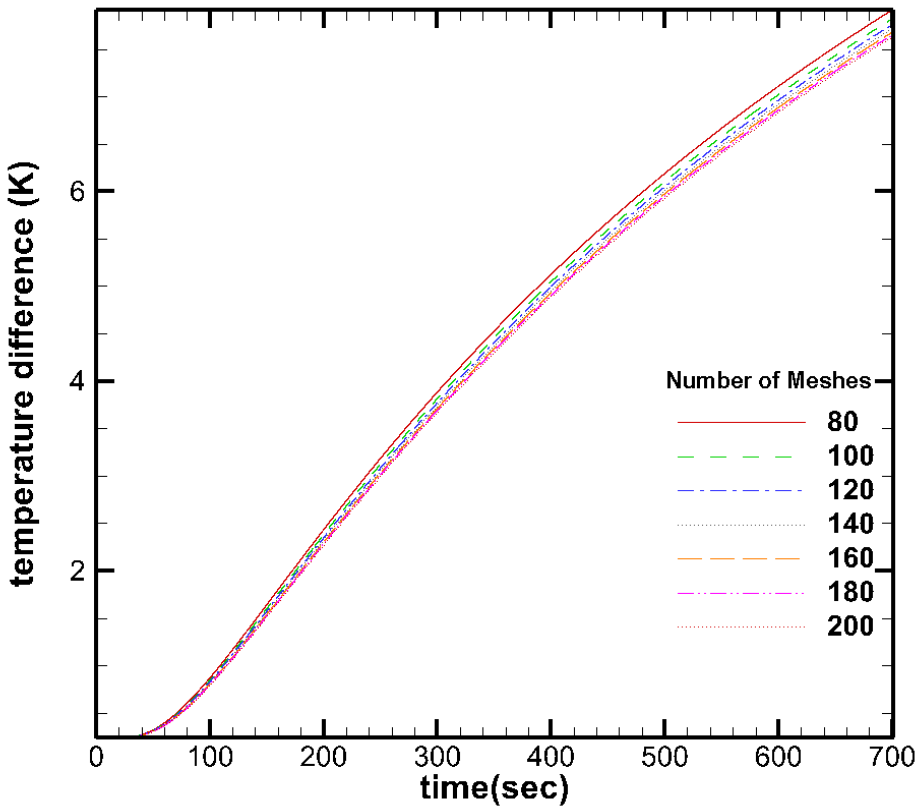

Figure 4-4. Mesh independent study of numerical solution for the iron-silica chain-structure for a/L = 0.015

In Figure 4-5, the dimensionless temperature of thermocouples of 1 and 2 (see Figure 4-3a) is shown as a function of the ratio a/L where a and L represent the material 1 thickness and the cell radius respectively. A decrease in a/L value corresponds to an increase in the frequency of the appearance of material 1 for a fixed volume of the sample. Figure 4-5 shows that as the a/L decreases (or frequency of appearance increased) the thermocouple 1 and 2 measurments merged to each other when a/L < 0.042. These results suggest that at high frequency of appearance for k_1/k_2=3, the temperature field is insensitive to the anisentropic media. Thus, an average thermal conductivity can be used to simulate the heat distribution within the media.

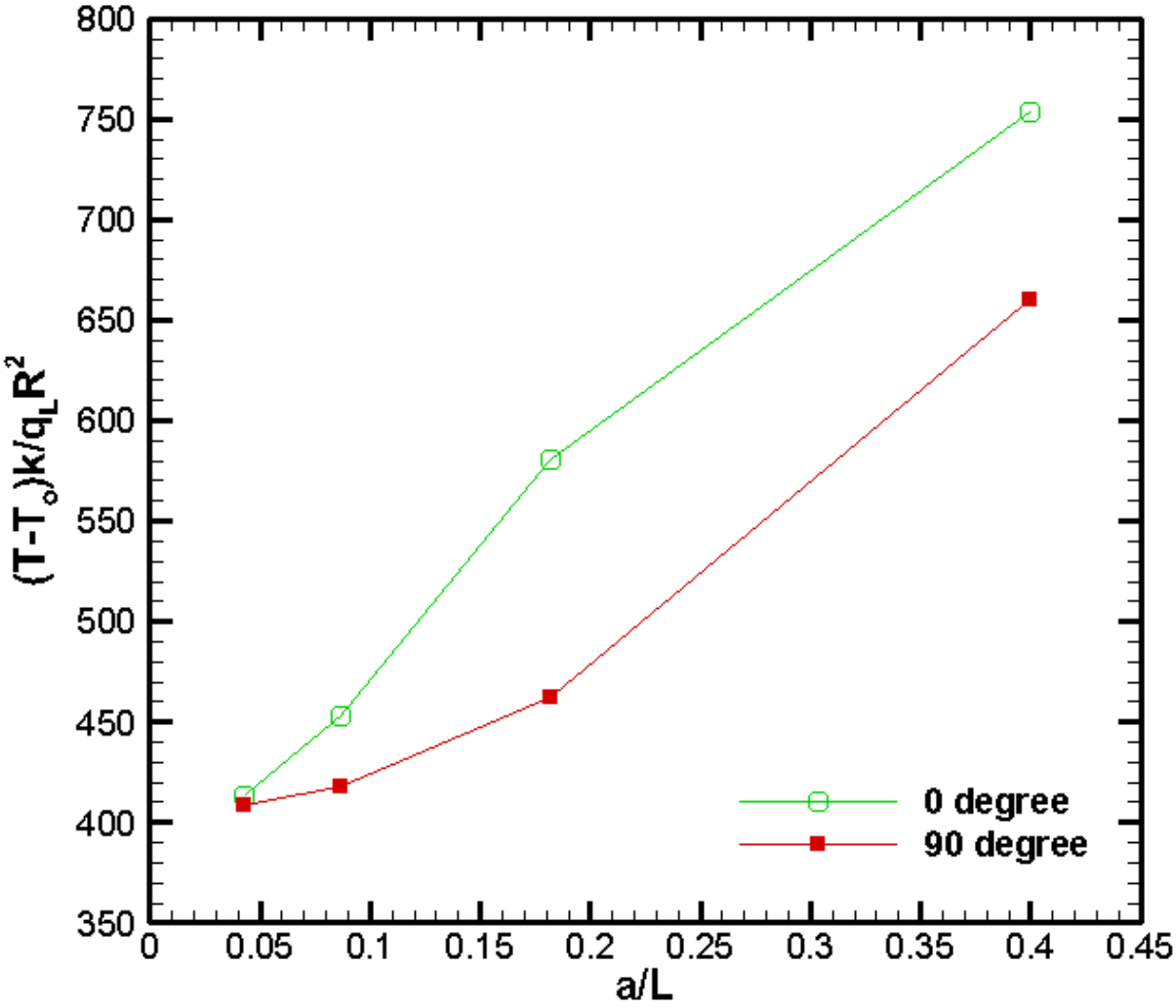

Figure 4-5. The dimensionless temperature as a function of a/L of chains appearance for points 1 and 2 and k_1/k_2=3

In order to ensure that this conclusion can be generalized for all the cases, the same numerical simulation is performed for different thermal conductivity ratios ($k_1/k_{2)}$. Figure 4-6 shows the dimensionless temperature as a function of of a/L at the same radial position at θ=0 and 90° when the thermal conductivity ratio is 50. In this case, the similar trend is observed where the temperature measured at points 1 and 2 merge together for high frequency of appearance of material 1 and 2 when a/L < 0.025.

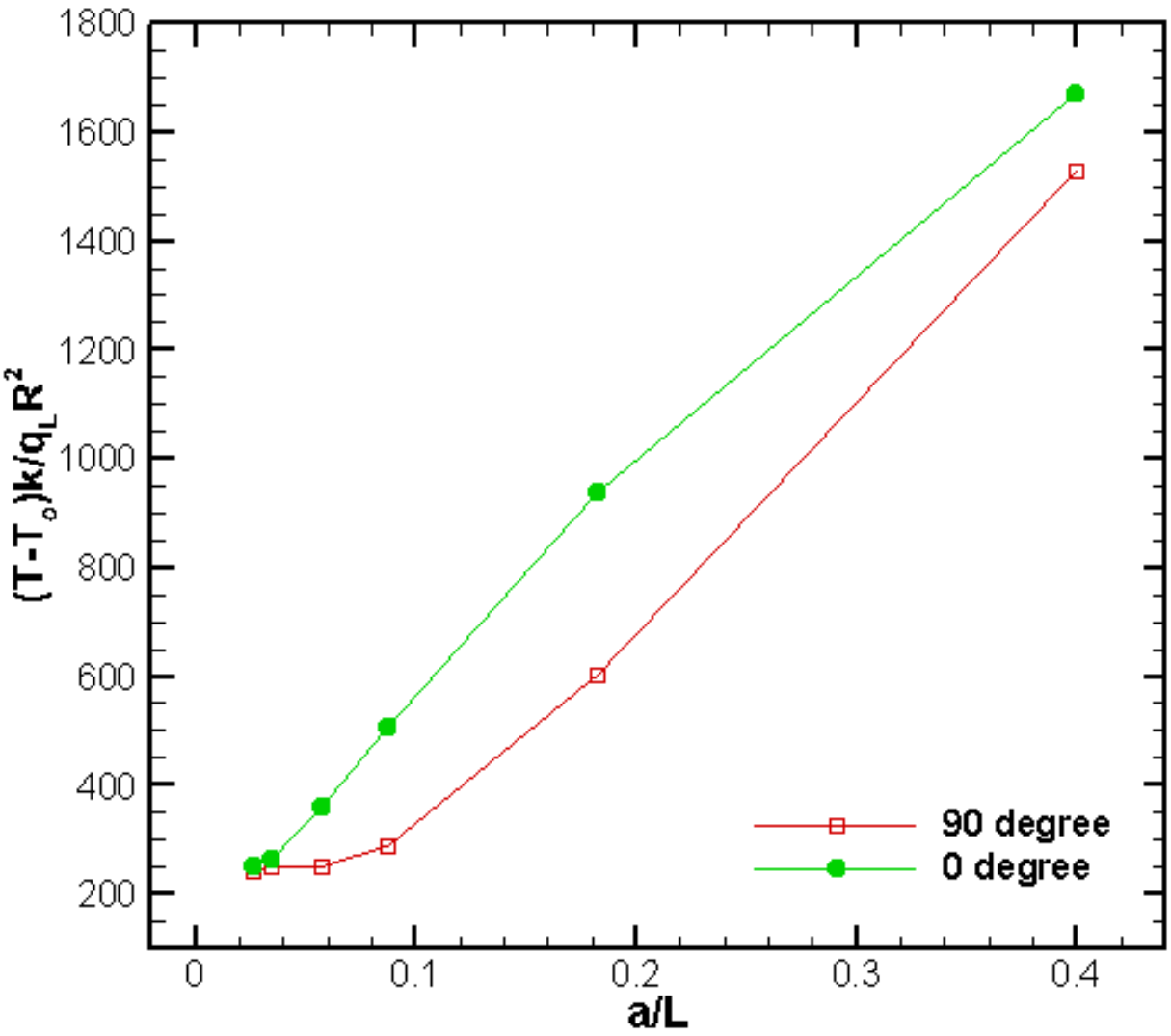

Figure 4-6. The dimensionless temperature as a function of a/L of chains appearance for two orthogonal fixes radial positions of points 1 and 2 and k_1/k_2=50

Figure 4-7 shows the simulation results variation of the heat flux and temperature for different angles at the fixed radial to the heat source. This figure shows that, for high frequency of iron-silica chains appearance (see Figure 4-3), there is no significant change in radial heat flux and temperature distribution along the azimuthal direction (Figure 4-7 and Figure 4-8).

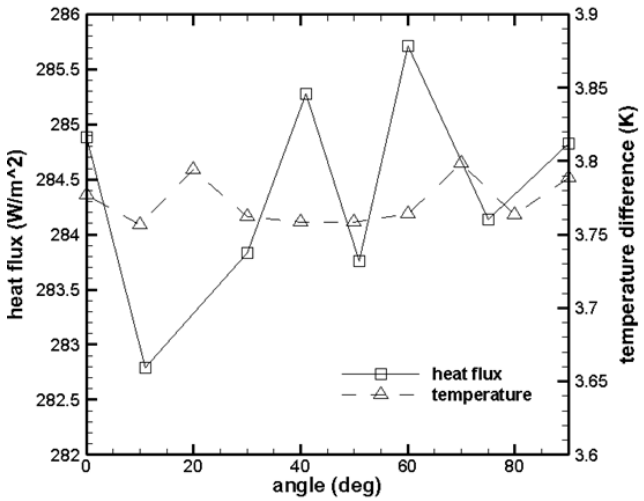

Figure 4-7. Azimuthal radial heat flux and relative temperature (compared to room temperature) of iron-silica distribution for a fixed radial position

The temperature contour has been also plotted after 350 second in Figure 4-8. Therefore, as was discovered in previewed figures, for high frequency of appearance of material 1 and 2 the isothermal lines are located on circles where their distance to the heat source are unchanged.

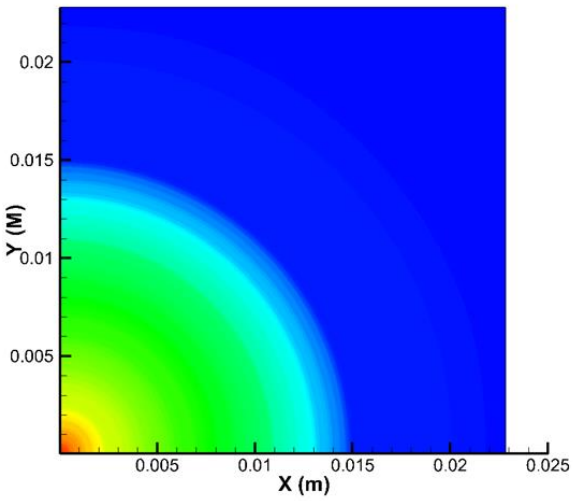

Figure 4-8. Temperature contour horizontal chains at 350 seconds and $k_1/k_2=3$

CHAPTER 5
CONCLUSIONS AND FUTURE WORKS

5.1 Conclusion

The experimental results showed that, when the magnetic field direction was perpendicular to the hot wire axis, the maximum thermal conductivity reduction was 12% in compared to the case without any magnetic field. It was suggested that the magnetic field organized the iron chains in the normal direction of hot wire surface and repulsive force between chains, increases the structure porosity. Both of these effects will limit the heat flux penetration from the hot wire to the media and results in a lower thermal conductivity. On the other hand, when the magnetic field switched to the parallel direction to hot wire axis, the radial thermal conductivity decreased by 11 % due to decreased contact between iron particles in the radial direction. Table and Figure 5-1 show the average calculated value of thermal conductivity of iron-silica porous structure with/without magnetic field measured by exposed thermocouples for two different amounts of heat fluxes values and Figure 5-2 shows the thermal conductivity of iron-silica powder while the porosity was changing.

Table 5-1. Average thermal Conductivity and the slope of temperature vs. log of time graph with different values of heat fluxes and magnetic field orientations.

Heat flux (W)	Average thermal conductivity without magnetic field (W/m K)	Average thermal conductivity with horizontal magnetic field (W/m K)	Average thermal conductivity with vertical magnetic field (W/m K)
3.8	0.212	0.188	0.190
7.4	0.211	0.193	0.196

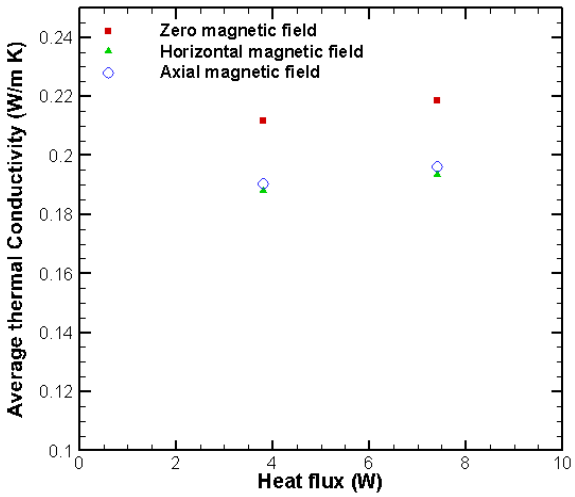

Figure 5-1. Average thermal conductivity of iron-silica porous structure for different heat fluxes/magnetic field orientations

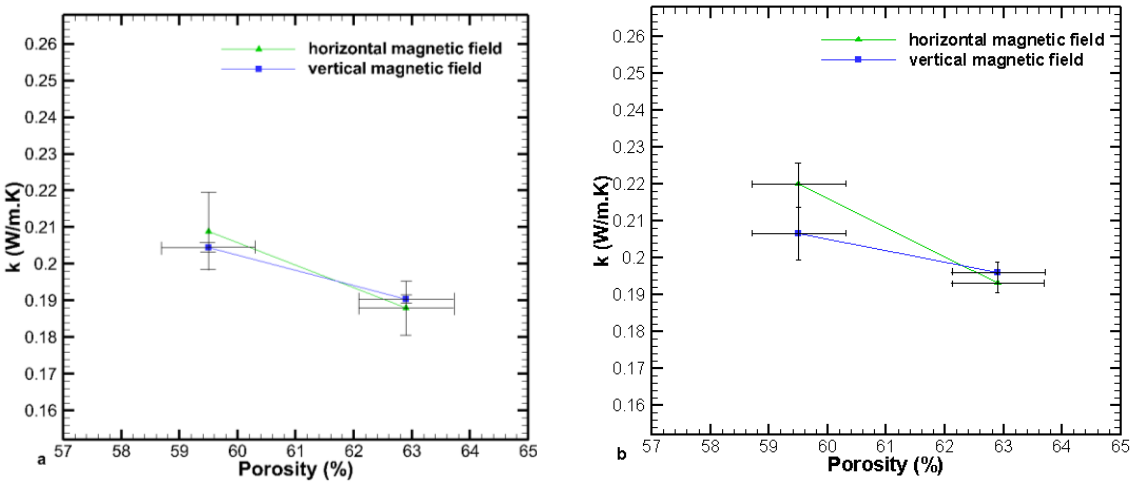

Figure 5-2. Thermal conductivity vs prosity. A) 3.8 watts heat flux. B) 7.3 watts heat flux.

Also the numerical simulation shows that, the temperature of unchanged radial positions from the heat source merges for anisentropic media, if the frequency of appearance of materials is high enough. Moreover, this study suggests that, for simulation purposes, we might use the average conductivity values (reported in Figure 5-1) to find the temperature distribution inside the media. It was both numerically and

experimentally verified that applying the magnetic field does not have any significant effect on the behavior of the propagation of heat in any direction. Therefore, it is concluded that the change in the thermal conductivity of MSPS is mainly due to the increase of porosity. Further investigations need to be done for the same structure at high temperature to evaluate the sintering effect on the thermal conductivity.

5.2 Future Works

To further explain these below items can be studied in future studies:

1. Investigation on effect of higher temperature on thermal conductivity of the sintered pours structure
2. Investigation of effect of different orientation/flux magnetic field on thermal conductivity of the packed bed reactor
3. Investigation on effect of higher temperature on thermal conductivity of MSPS
4. Computing the convective heat transfer coefficient by a similar method and investigation of the influence due to magnetic field presence
5. Validating the results with numerical simulation

REFERENCES

[1] Ayyoub M. Mehdizadeh, James F. Klausner, Amey Barde, Renwei Mei, Enhancement of thermochemical hydrogen production using an iron–silica magnetically stabilized porous structure, International Journal of Hydrogen Energy, Issue 11, 2012;37: 8954-8963.

[2] Subbojin V.I. Haritonov V.V , Thermophysics of cooled laser mirrors. Teplofizika Vys. Temp. (1991); 29 (2):365–375.

[3] Jeigarnik U.A, Ivanov F.P, Ikranikov N.P Experimental data on heat transfer and hydraulic resistance in unregulated porous structures Teploenergetika (1991); (2):33–38.

[4] Lage J.L, Weinert A.K, Price D.C, Webe R.M. r Numerical study of a low permeability microporous heat sink for cooling phased-array radar systems Int. J. Heat Mass Transfer. 1996; 39 (17):3633–3647.

[5] Chrysler G.M, Simons R.E, An experimental investigation of the forced convection heat transfer characteristics of fluorocarbon liquid flowing through a packed-bed for immersion cooling of microelectronic heat sources, in: AIAA/ASME Thermophysics and Heat Transfer Conference, Cryogenic and Immersion Cooling of Optics and Electronic Equipment, , 1990. ASME HTD-131: 21–27.

[6] Kuo S.M, Tien C.L, Heat transfer augmentation in a foam-material filled duct with discrete heat sources, in: Intersociety Conference on Thermal Phenomena in the Fabrication and Operation of Electronic Components, IEEE, New York, 1988:87–91.

[7] Ayyoub M. Mehdizadeh, James F. Klausner, Amey Barde, Renwei Mei, Enhancement of thermochemical hydrogen production using an iron–silica magnetically stabilized porous structure, International Journal of Hydrogen Energy, Issue 11, 2012;37: 8954-8963.

[8] Singh Ramvir, Bhoopal R.S, Kumar Sajjan, Prediction of effective thermal conductivity of moist porous materials using artificial neural network approach, Building and Environment, 12, December 2011: 46;2603-2608.

[9] Nakamura M.T, Tanahashi D., Ohsasa T.K, Suguyama S, Heat transfer in a packed bed with gas liquid concurrent upflow Heat Transfer: Japanese Research, 1981;10 : 92–99.

[10] Sokolov V.N, Yablokova M.A, Thermal conductivity of a stationary granular bed with upward gas-liquid flow, Journal of Applied Chemistry USSR (Zh. Prikl. Khim.), 1983;56: 551–553.

[11] Gutsche S, Wild G, Roizard C, Midoux N, & Charpentier J. C, Heat transfer phenomena in packed bed reactors with co current up flow of gas and liquid. Proceedings of the fifth conference on applied chemical unit operations and processes, Veszprém, Hungary, 1989: 402–408.

[12] Lamine A.S, M.T. Collı́ Serrano, G. Wild Hydrodynamics and heat transfer in packed bed with cocurrent upflow, Chemical Engineering Science, 1992;47:3493–3500.

[13] Lamine A.S, M.T. Collı́ Serrano, G. Wild Hydrodynamics and heat transfer in packed bed with cocurrent upflow Chemical Engineering and Processing, 1992;6: 385-394.

[14] Hall R.O.A, Martin D.G, The thermal conductivity of powder beds. A model, some measurements on UO2 vibro-compacted microspheres, and their correlation] referred to as HM, and the model of Zehner, Bauer and Schlünder [Effective radial thermal conductivity of packings in a gas flow. Part II, Thermal conductivity of the packing fraction without gas flow, Int. Chem. Eng, 1978;18:189–204.

[15] Tsotsas E, Martin H., Thermal conductivity of packed beds: a review, Chem. Eng. Process,1987; 22:19–37.

[16] Fundamenski W, Gierszewski P, Heat transfer correlations for packed beds Fusion Technol,1992; 21:2123.

[17] Xu M, Abdou M.A, Raffray A.R, Thermal conductivity of a beryllium gas packed bed Fusion Eng. Des,1995; 27:240–246.

[18] Adnani P, Modeling of transport phenomena in porous media, PhD thesis, University of California, Los Angeles, CA, 1991.

[19] Hammerschmidt U. and Sabuga W, Transient Hot Wire THW Method: Uncertainty Assessment, Int. J. Thermophys., 2000: 21; 1255–1278.

[20] De Groot, J. J, Kestin, J, and Sookiazian, H, Instrument to Measure the Thermal Conductivity of Gases, Physica Amsterdam, 1974: 75; 454–482.

[21] Healy J. J, de Groot J. J, and Kestin J, The Theory of the Transient Hot-Wire Method for Measuring Thermal Conductivity, Physica C, 1976: 82; 392–408.

[22] Kestin, J, and Wakeham, W. A, A Contribution to the Theory of the Transient Hot-Wire Technique for Thermal Conductivity Measurements, Physica A, 1978: 92; 102–116.

[23] Assael, M. J, Dix, M, Gialou, K, Vozar, L, and Wakeham, W. A., Application of the Transient Hot-Wire Technique to the Measurement of the Thermal Conductivity of Solids, Int. J. Thermophys., 2002: 23; 615–633.

[24] Vozar, L, A computer-controlled apparatus for thermal conductivity measurement by the transient hot wire method. Journal of Thermophysics and heat transfer,1996 :13 (4);474-480.

[25] Tye, R.P.(ed), Thermal Conductivity, 1969:2. London: Academic Press

[26] Nagasaka, Y, and Nagashima, A, Absolute Measurement of the Thermal Conductivity of Electrically Conducting Liquids by the Transient Hot-Wire method, J. Phy. E: Sci. Instrum., 1981:14; 1435-40.

[27] Johns, A. I, Scott, A. C., Watson, J.T.R, Ferguson, D., and Clifford, A. A, Measurement of the thermal conductivity of gases by the transient hot wire method. Philosophical Transactions of the Royal Society of London. Series A, Mathematical and Physical Sciences. 1988: A 325; 295-356.

[28] Roder, Hans M, A transient hot wire thermal conductivity apparatus for fluids. Journal of Reasearch of the National Bureau of Standards, 1981: 86(5);457-493

[29] Assael, M. J, Chen, C.-F., Metaxa, I, and Wakeham, W. A, Thermal Conductivity of Suspensions of Carbon Nanotubes in Water, Int. J. Thermophys., 2004: 25; 971–985.

[30] Yamasue, E, Susa, M, Fukuyama, H, and Nagata, K, Nonstationary Hot-Wire Method with Silica-Coated Probe for Measuring Thermal Conductivities of Molten Metals, Metallurgical and Materials Transactions A, 1999: 30:1971-79.

[31] Perkins, Richard A. Measurement of the Thermal Properties of Electrically Conducting Fluids using Coated Transient Hot Wires, Presented at the 12th Symposium on Energy Engineering Sciences, Dept. of Energy, CONF-9404137, 1994: 90-97.

[32] Yu, Wenhua, Hull, John R, and Choi. Stephen U. S., Stable and Highly Conductive Nanofluids – Experimental and Theoretical Studies, The 6th ASME – JSME Thermal Engineering Conference, Hawaii Islands, Hawaii., 2003.

[33] Jwo, C. S, Teng T. P., Hung C. J., and Guo Y. T, Research and Development Device for Thermal Conductivity of Nanofluids, Journal of Physics, Conference Series , 13: 55-58.

[34] Ma, Jack Jeinhao, M.S. Thesis: Thermal Conductivity of Fluids Containing Suspensions of Nanometer-Sized Particles, Massachusetts Institute of Technology, 2006.

BIOGRAPHICAL SKETCH

Samaun Nili was born in 1987 in Miami Florida and moved overseas at the age 7 due to his father's professions. He completed his elementary as well as high school educations in Tehran- Iran. Since Samaun had technical and mathematical oriented mind, he chose mathematics and physics as his major in pre-university studies.

His achievements from elementary through pre-university were outstanding. He took a national university entry examination and he got the eligibility to take any engineering major in the top ten universities in Tehran but he chose mechanical engineering as his major. Samaun completed his undergraduate studies in 2009 with an excellent performance from Azad University in Tehran Iran. Then he decided to move back to Florida for continuation of his higher educations in mechanical engineering.

Samaun was admitted and started his first semester at Florida Atlantic University (FAU) in spring of 2011 as a graduate student, majoring in mechanical engineering. During this time he realized that the Department of Mechanical and Aerospace Engineering at the University of Florida (UF) would serve his purpose the best therefore, he applied and was accepted into the Department of Mechanical and Aerospace Engineering in UF for fall of 2011 and completed his requirement for his M.S. degree in spring term of 2013 at the UF.

Samaun thinks there is much more to learn in the field of mechanical engineering and for that reason he is trying to enter to PhD program preferably at the University of Florida which, he is anxiously waiting to receive his admission.